AIAA JOURNAL
Vol. 45, No. 5, May 2007

Large-Eddy Simulations of Subharmonic Transition in a Supersonic Boundary Layer

Steffen Stolz,* Philipp Schlatter,† and Leonhard Kleiser
Institute of Fluid Dynamics, ETH Zürich, 8092 Zürich, Switzerland

DOI: 10.2514/1.15048

We investigate the performance of two recently developed subgrid-scale models, the approximate deconvolution model and the high-pass filtered Smagorinsky model, in large-eddy simulations of laminar-turbulent transition in a supersonic boundary layer. Subharmonic transition in a boundary layer at a freestream Mach number of 4.5 and a Reynolds number (based on initial displacement thickness) of 10,000 is considered, which has been studied previously in detail by direct numerical simulations. For computational efficiency, the temporal simulation approach has been adopted. The discretization is based on Fourier collocation and various high-order finite difference schemes in the wall-parallel and wall-normal directions, respectively. Large-eddy simulations results are assessed by comparing statistical and instantaneous quantities during transition with data obtained from a sufficiently resolved direct numerical simulation. The results show that the large-eddy simulations accurately reproduce the direct numerical simulations data from the slightly disturbed laminar flow through transition into the turbulent stage, with a computational effort of two orders of magnitude less than the direct numerical simulations. Both subgrid-scale models are formulated locally in space and in a fully three-dimensional manner and do not need an ad hoc adaptation to nonturbulent or near-wall regions.

Nomenclature

A_N	=	amplitude of noise disturbance
A_{2D}	=	amplitude of two-dimensional wave disturbance
a	=	speed of sound
C_f	=	skin-friction coefficient
$C^{\mathrm{HPF}}_{S,\omega_c}$	=	HPF model coefficient
c_v, c_p	=	specific heat coefficient at constant volume, pressure
E	=	total energy
F	=	generic flux function
G, G_i	=	primary low-pass filter (in direction x_i)
H	=	high-pass filter
H_{12}	=	shape factor
I	=	identity operator
L_0	=	reference length
M	=	Mach number
m^{HPF}_{ij}	=	modeled subgrid-scale stresses
N	=	deconvolution order
Pr	=	Prandtl number
Pr_t	=	turbulent Prandtl number
p	=	pressure
Q_N	=	deconvolution filter
q_i	=	heat flux caused by conduction
Re	=	computational Reynolds number
S_{ij}	=	strain rate tensor
T	=	temperature
t	=	time
U	=	streamwise velocity component
u_i	=	velocity components
x_i	=	spatial coordinates
α	=	streamwise wave number
α_i	=	subgrid-scale terms in energy equations
β	=	splitting parameter for entropy splitting
β_i	=	nonlinearity due to viscous stresses
γ	=	c_p/c_v
Δ	=	filter width
Δ_i	=	grid spacing in direction x_i
Δ_t	=	time interval
δ_{ij}	=	Kronecker delta
δ_0	=	99% boundary-layer thickness
δ_1	=	displacement thickness of the boundary layer
δ_2	=	momentum thickness of the boundary layer
μ	=	dynamic viscosity
ρ	=	density
σ_{ij}	=	subgrid-scale stresses
τ_{ij}	=	components of the shear-stress tensor
χ	=	relaxation coefficient
Ψ	=	state vector
ω	=	wave number
ω_c	=	filter cutoff wave number
ω_n	=	numerical cutoff wave number
$*$	=	convolution operator
$\langle\cdot\rangle$	=	average

Subscripts

∞	=	freestream quantity

Superscripts

$*$	=	dimensional quantity
$\tilde{(\cdot)}$	=	Favre average
$(\cdot)''$	=	Favre fluctuation
$\check{(\cdot)}$	=	computed according to definition with filtered variables
$\check{(\cdot)}^*$	=	computed according to definition with deconvolved variables
$\bar{(\cdot)}$	=	filtered quantity
$\hat{(\cdot)}$	=	Fourier transform (transfer function)
$(\cdot)^*$	=	deconvolved (defiltered) quantity

Received 10 December 2004; revision received 26 September 2006; accepted for publication 26 December 2006.

*Currently Philip Morris Research Center, CH-2000 Neuchâtel, Switzerland; steffen.stolz@pmintl.com.

†Currently KTH Mechanics, SE-100 44 Stockholm, Sweden; pschlatt@mech.kth.se.

I. Introduction

THE majority of numerical studies in the literature on laminar-turbulent transition have focused on incompressible flows.

However, in many cases, it is crucial to include compressibility effects, in particular, when dealing with high-speed flows. Transition in compressible flows is known to be substantially more complex than in incompressible flows [1–3]. Whereas in a subsonic compressible boundary layer the stability characteristics and routes to turbulence are qualitatively similar to those observed in incompressible flows, in supersonic boundary layers above Mach numbers M of about two, multiple unstable maxima appear in the stability diagram. The regions around the maxima are usually termed the Mack modes; however, from a mathematical point of view, they belong to the same normal mode [4]. In particular, the second Mack modes belong to an (inviscid) acoustic instability, and for Mach numbers above about four, their growth rate can exceed that of the unstable Tollmien–Schlichting (TS) wave (first mode). Generally, in higher Mach-number boundary-layer flows, the most unstable first modes are oblique waves, in contrast to the second mode, for which the highest growth rate occurs for two-dimensional waves [5].

A number of direct numerical simulations (DNS) of transition in compressible boundary layers have been published (see, for example, [6,7] (and the references therein) and the review by Rempfer [8]). The subharmonic transition process in a Mach 4.5 boundary layer, starting from the weakly disturbed laminar flow up to fully developed turbulence, has been simulated previously in temporal DNS by Adams [9], Adams and Kleiser [10] and Mielke and Kleiser [11]. Detailed analysis of the flow development has been undertaken and mechanisms of transition were identified, including the role of Λ vortices, various shear layers, and hairpin vortices in the breakdown stage of transition. Consistent with experimental observations, an overshoot of the skin friction during the later transitional stages beyond the turbulent value has been observed. In the present work, we will focus on the specific case initiated by Adams [9].

The application of large-eddy simulations (LES) to laminar-turbulent transition has only recently become a topic of active research. These studies showed that when using appropriate subgrid-scale (SGS) models, the necessary resolution for transition simulations can be lowered significantly, compared with the DNS (see, for example, Germano et al. [12] and Meneveau et al. [13]). It should be noted that transitional flows are substantially different from turbulent flows, because there is, for example, no fully developed energy cascade and the slow growth of various instability modes and their interaction with the base flow needs to be resolved or modeled appropriately. Furthermore, the SGS model has to cope with the simultaneous presence of laminar, various transitional and fully turbulent flow regions within the computational integration domain, and with the specific effects of solid walls [14].

Unlike for incompressible flows, only a few LES of laminar-turbulent transition in supersonic flows have been performed. For example, El-Hady and Zang [15] used the dynamic mixed model [16] with a dynamic eddy-diffusivity ansatz for the simulation of the transition process in a zero-pressure gradient boundary layer at a Mach number of $M = 4.5$. To avoid instabilities from the dynamic procedure [12], they employed averaging of the dynamic coefficients over wall-parallel planes, which does not result in a spatially local formulation of the SGS model. Normand and Lesieur [17] performed LES of laminar-turbulent transition in a boundary-layer flow over a flat plate at $M = 0.5$ and $M = 5$ using the structure-function model of Métais and Lesieur [18], in which only contributions to the structure-function normal to the mean shear were considered. Ducros et al. [19] proposed a modified version of the structure-function model [18], the filtered-structure-function (FSF) model, and applied it to LES of transition to turbulence in a spatially developing boundary layer over a flat plate at $M = 0.5$. Similarly, Shan et al. [20] employed the FSF model for LES of a transitional boundary layer at $M = 4.5$. For all SGS models based on the structure function [17,19,20], the structure function itself is computed in wall-parallel (two-dimensional) planes only, which does not result in a fully three-dimensional formulation of the SGS model. Recently, Teramoto [21] performed an LES study of a transitional Mach 2 boundary layer exposed to an incident shock wave using a selective mixed-scale SGS model. He concluded that the gross features of the boundary-layer development, including separation and reattachment, were predicted correctly, but his grid resolution was too coarse to resolve the breakdown of the large-scale transitional structures.

Transition simulations of spatially evolving flows can either be performed using the spatial or the temporal framework. In the temporal framework, only a part of the physical domain (for harmonic excitation, usually one wavelength of the primary disturbance) is simulated in time, in a moving frame of reference, rather than in space. The boundary condition in the streamwise direction can thus be chosen as periodic, rendering the streamwise direction homogeneous. The main advantages of the temporal simulation approach are that the domain can be chosen much smaller in the streamwise direction than for a corresponding spatial simulation and, due to the periodic boundary conditions, neither inflow nor outflow need to be specified. Additionally, more efficient numerical methods can be applied. Fully resolved spatial simulations are at least an order of magnitude more expensive in terms of computer time, in particular, if part of the developed turbulent region is also included in the domain and simulated accurately.

During the first weakly nonlinear and slowly evolving stages of transition, the temporal approach is well justified [22], even in the case of spatially developing flows (e.g., boundary layers). However, there are differences during the highly intermittent later transitional stages concerning the evolution of the physical flow structures [23,24]. Furthermore, using the temporal approach, only forced transition can be simulated, that is, the instability mechanism is selected by the initial condition ($t = 0$). Spatial simulations allow greater flexibility, because receptivity effects can also be taken into account (e.g., bypass transition [25]).

It has been shown in a recent study [14,24] that for the purpose of evaluating appropriate SGS modeling of forced transition in incompressible channel flows, the temporal framework is sufficient. In that work, simulation results were obtained for the same physical test case by using both the temporal and spatial approach. In particular, the impact of the SGS model on the results was very similar with both simulation types.

The aim of the present work is to demonstrate that LES using the approximate deconvolution model (ADM) or high-pass filtered Smagorinsky model (HPF-SM) subgrid-scale models are also able to accurately represent the complete transition process in compressible high-speed flow, in particular, a supersonic boundary layer. To allow for an accurate assessment of the different LES methods for compressible transitional flows, in the present study, well-resolved DNS results serve as a reference. To this end, a DNS similar to those of [10,11] was performed. Different from the previous DNS, however, a higher resolution in all spatial directions was employed, and interpolation necessary to gradually increase the grid resolution during the simulation was avoided by using a grid fine enough to capture the laminar-turbulent transition from the beginning of the simulation.

The physical processes during the transitional breakdown for this type of flow have already been addressed in detail in the previously mentioned studies [9,10] and are not the topic of the present contribution. Rather, the predictions of LES are assessed quantitatively, and differences and specific modeling issues are pointed out.

For the LES we employ the approximate deconvolution model (ADM) [26–28] and the high-pass filtered (HPF) Smagorinsky model [29–31]. ADM has already been applied to a number of different flows, including incompressible transitional [32,33] and turbulent [27] channel flow, compressible homogeneous isotropic turbulence [26], supersonic boundary-layer flow [34] and the flow along a compression ramp [28]. The HPF Smagorinsky model has been used in incompressible transitional and turbulent channel flow [30] with a detailed analysis of the energy transfer [35]. Compressible spatially developing turbulent high-speed boundary-layer flow has been simulated successfully by Stolz [29]. For both SGS models, no special near-wall treatment (such as van Driest wall-damping functions) for a correct prediction of the viscous sublayer of wall-bounded turbulent flows or an intermittency function for computation of laminar-turbulent transition [36] was found

necessary. Moreover, in contrast to previous LES, both SGS models are formulated locally in space and in a fully three-dimensional manner. The simulations using the HPF Smagorinsky model were performed using a fixed model coefficient (i.e., no dynamic procedure was necessary).

II. Compressible Governing Equations and Numerical Method

We employ the nondimensional continuity, momentum, and energy equations for a compressible fluid. The nondimensionalization is done with the dimensional reference quantities U_∞^*, ρ_∞^*, and T_∞^*, which are chosen as the freestream quantities in the following, and the reference length scale L_0^* is chosen as the initial displacement thickness δ_1. The equations written in conservation form are

$$\frac{\partial \rho}{\partial t} + \frac{\partial}{\partial x_j}(\rho u_j) = 0 \tag{1}$$

$$\frac{\partial \rho u_i}{\partial t} + \frac{\partial}{\partial x_j}(\rho u_i u_j + p\delta_{ij} - \tau_{ij}) = 0 \tag{2}$$

$$\frac{\partial E}{\partial t} + \frac{\partial}{\partial x_j}(E u_j + p u_j - \tau_{ij} u_i + q_j) = 0 \tag{3}$$

where the viscous stresses are τ_{ij}, the heat flux is q_j, the pressure calculated from the total energy E and the kinetic energy is

$$p = (\gamma - 1)E - \frac{\gamma - 1}{2}\rho u_k u_k$$

the Reynolds number is $Re = \rho^* U_\infty^* L_0^*/\mu^*$, and the Prandtl number is Pr. The viscosity μ^* is calculated according to Sutherland's law. We also assume the thermal equation of state for perfect gases to be valid, $\gamma M_\infty^2 p = \rho T$, where $M_\infty = U_\infty/a_\infty$ is the freestream Mach number and γ is the ratio of specific heats.

For the reference DNS and the LES with ADM, the same numerical discretization was employed as in the earlier DNS by Adams [9], Adams and Kleiser [10], and Mielke and Kleiser [11], consisting of a symmetric sixth-order (at inner points) compact finite difference scheme [37] for discretization in the wall-normal direction and a Fourier-collocation scheme for the periodic streamwise and spanwise directions. The second derivatives in the viscous term were discretized with sixth-order compact finite difference schemes directly, instead of repeated application of the first derivative schemes.

For stability reasons, the LES applying the HPF Smagorinsky model were performed using a high-order numerical scheme as proposed by Sandham et al. [38], consisting of a fourth-order central explicit finite difference scheme for the wall-normal direction, satisfying a summation-by-parts condition [39] and a fourth-order central scheme for the second derivatives [38,39]. Furthermore, an entropy-splitting approach that splits Eulerian fluxes into conservative and nonconservative parts [40,41] was employed. A splitting parameter $\beta = 6$ is used such that six of seven Eulerian fluxes are computed in their conservative form and one of seven is in the entropy-splitting form [29]. The parameter is thus within the region $2 \leq \beta \leq 8$, as proposed by Sandham et al. Similar to the viscous terms, second derivatives are also discretized directly for the eddy-viscosity model, to further reduce odd–even oscillations.

The equations are integrated in time with an explicit low-storage third-order Runge–Kutta scheme [42] for all simulations. Note that the spatial discretization schemes described earlier do not introduce additional artificial dissipation. Moreover, simulations with the considered numerical schemes were found to be unstable on coarse grids without SGS model, demonstrating the necessity of the SGS model for the considered case.

As shall be detailed next, the influence of the different numerical schemes was investigated by performing various LES using ADM and the HPF Smagorinsky model.

III. Subgrid-Scale Models

In this section, the two different subgrid-scale models used in the large-eddy simulations are presented in their compressible formulation.

A. Approximate Deconvolution Model

For simplicity, we demonstrate the ADM approach [26,28] with a generic one-dimensional transport equation for $\Psi \in \{\rho, \rho u_1, \rho u_2, \rho u_3, E\}$, representing Eqs. (1–3), respectively,

$$\frac{\partial \Psi}{\partial t} + \frac{\partial F(\Psi)}{\partial x} = 0 \tag{4}$$

In this equation, the corresponding functional expressions for the flux $F(\Psi)$ are to be used, and corresponding additional terms of the flux divergence have to be added for higher dimensions.

We employ explicit discrete filter operations on a grid function u_i, where $u_i = u(x_i)$ and $\{x_i\}$ is a (not necessarily equidistant) mesh, defined in one dimension as

$$G * u|_i = \bar{u}_i := \sum_{j=-\nu_l}^{\nu_r} \alpha_j u_{i+j} \tag{5}$$

and consider five-point discrete filters with $\nu_l + \nu_r = 4$ for inner grid points. The five coefficients α_j are determined from conditions given by Stolz et al. [27], resulting in filters with a cutoff wave number $\omega_c \approx 2\pi/3$, which is defined by $|\hat{G}(\omega_c)| = 1/2$, where $\hat{G}$ denotes the transfer function of G in Fourier space. For a three-dimensional domain, the filter is applied in each coordinate direction successively, yielding $\bar{u}(x_1, x_2, x_3) = G_1 * G_2 * G_3 * u$.

Applying the filter operation (5) to the one-dimensional transport equation (4), we obtain

$$\frac{\partial \bar{\Psi}}{\partial t} + \overline{\frac{\partial F(\Psi)}{\partial x}} = 0 \tag{6}$$

where the effect of the grid discretization has been omitted for ease of notation. Resolved scales can be recovered to some extent by an approximate inversion of the filter (5), resulting in an approximation Ψ^* of the unfiltered solution Ψ on the grid $\{x_i\}$ [26]. Assuming that the filter G has an inverse, the inverse operator can be expanded as an infinite geometric series of filter operators. Filters with compact transfer functions are noninvertible, but a regularized inverse operator Q_N can be obtained by truncating the geometric series at some deconvolution order N, for example, $N = 5$, obtaining a regularized approximation [26] of G^{-1}:

$$Q_N := \sum_{\nu=0}^{N} (I - G)^\nu \approx G^{-1} \tag{7}$$

where I is the identity operator. The approximate deconvolution Ψ^* is defined by applying the approximate deconvolution operator Q_N to $\bar{\Psi}$:

$$\Psi^* := Q_N * \bar{\Psi} \tag{8}$$

Here, we model the filtered flux term directly by replacing the unfiltered quantities Ψ in the filtered flux term with the approximate deconvolution Ψ^*:

$$\overline{\frac{\partial F(\Psi)}{\partial x}} \approx \overline{\frac{\partial F(\Psi^*)}{\partial x}}$$

However, the effect of nonrepresented scales $|\omega| > \omega_n$ on the resolved scales cannot be modeled by just replacing the unfiltered Ψ with Ψ^* in the flux term [28]. To model the energy transfer from scales $|\omega| \leq \omega_n$ to scales $|\omega| > \omega_n$, energy is drained from the range $\omega_c < |\omega| \leq \omega_n$ by subtracting a relaxation term $\chi_\Psi(I - Q_N * G) * \bar{\Psi}$, with $\chi_\Psi > 0$, from the right-hand side, which results in the modeled equation:

$$\frac{\partial \bar{\Psi}}{\partial t} + \overline{\frac{\partial F(\Psi^*)}{\partial x}} = -\chi_\Psi(\bar{\Psi} - \bar{\Psi}^\star) = -\chi_\Psi(I - Q_N * G) * \bar{\Psi} \quad (9)$$

The relaxation parameter χ_Ψ is determined dynamically from the instantaneous filtered solution [27,28]. For this determination, we consider the kinetic energy contained in the range $\omega_c < |\omega| \leq \omega_n$ and require that no energy should accumulate in this range during time advancement, to maintain a filtered solution $\bar{u}_i$ that is well-resolved by the scales in the range $|\omega| \leq \omega_c$. By construction, the relaxation term essentially acts in the range $|\omega| \geq \omega_c$, for which a finite difference discretization becomes inaccurate anyway.

According to Eq. (9), the following equations for the filtered conservative variables $\bar{\rho}$, $\overline{\rho u_i}$, $i = 1, 2, 3$, and $\bar{E}$ are obtained as

$$\frac{\partial \bar{\rho}}{\partial t} + \overline{\frac{\partial (\rho u_j)^\star}{\partial x_j}} = -\chi_\rho(\bar{\rho} - \bar{\rho}^\star) \quad (10)$$

$$\frac{\partial \overline{\rho u_i}}{\partial t} + \overline{\frac{\partial}{\partial x_j}\left((\rho u_i)^* \frac{(\rho u_j)^*}{\rho^*} + \check{p}^* \delta_{ij} - \check{\tau}^*_{ij}\right)} = -\chi_{\rho u}(\overline{\rho u_i} - \overline{\rho u_i}^*) \quad i = 1, 2, 3 \quad (11)$$

$$\frac{\partial \bar{E}}{\partial t} + \overline{\frac{\partial}{\partial x_j}\left(E^* \frac{(\rho u_j)^*}{\rho^*} + \check{p}^* \frac{(\rho u_j)^*}{\rho^*} - \check{\tau}^*_{ij} \frac{(\rho u_i)^*}{\rho^*} + \check{q}^*_j\right)} = -\chi_E(\bar{E} - \bar{E}^*) \quad (12)$$

The symbol $\check{}^*$ indicates that the respective quantities are computed according to their definition but are based on deconvolved variables.

Three different relaxation parameters χ_ρ, $\chi_{\rho u}$, and χ_E are used for the continuity, momentum, and energy equations, respectively. Because the relaxation parameters are computed dynamically from the instantaneous solution, ADM is parameter-free. Furthermore, it was shown that a variation of a relaxation parameter χ (considered to be constant in space and time) up to a factor of 8 has only a negligible effect on the results in incompressible channel flows [27]. A similar conclusion could also be drawn from LES of transitional channel flows [14].

B. High-Pass Filtered Eddy-Viscosity Models

For the LES using the high-pass filtered eddy-viscosity ansatz as a SGS model [29,30], we derive the filtered Navier–Stokes equations following Vreman [43] and neglect commutation errors due to a variable filter width. This results in the fundamental equations for the resolved conservative variables $\{\bar{\rho}, \bar{\rho}\tilde{u}_1, \bar{\rho}\tilde{u}_2, \bar{\rho}\tilde{u}_3, \check{E}\}$ being the filtered density, filtered momentum, and total resolved energy, respectively. Filtered quantities are indicated by $\bar{}$. Furthermore, Favre-filtered quantities, denoted by $\tilde{}$, are computed from a mass-weighted filtering operation $\tilde{\phi} = \overline{\rho\phi}/\bar{\rho}$, and quantities denoted by $\check{}$ are computed according to their definition but are based on filtered variables.

The filtered continuity and momentum equations and the equation for the total resolved energy $\check{E} = \bar{p}/(\gamma - 1) + \frac{1}{2}\overline{\rho u_i}\,\overline{\rho u_i}/\bar{\rho}$ are given by

$$\frac{\partial \bar{\rho}}{\partial t} + \frac{\partial \bar{\rho}\tilde{u}_j}{\partial x_j} = 0 \quad (13)$$

$$\frac{\partial \bar{\rho}\tilde{u}_i}{\partial t} + \frac{\partial}{\partial x_j}(\bar{\rho}\tilde{u}_i\tilde{u}_j + \bar{p}\delta_{ij} - \check{\tau}_{ij}) = -\frac{\partial \bar{\rho}\sigma_{ij}}{\partial x_j} + \beta_i \quad (14)$$

$$\frac{\partial \check{E}}{\partial t} + \frac{\partial}{\partial x_j}[(\check{E} + \bar{p})\tilde{u}_j - \check{\tau}_{ij}\tilde{u}_i + \check{q}_j] = -\alpha_1 - \alpha_2 - \alpha_3 + \alpha_4 + \alpha_5 - \alpha_6 \quad (15)$$

where the viscous stress tensor is $\check{\tau}_{ij}$. The subgrid-scale stresses and the subgrid-scale term due to the nonlinearity of the viscous stresses are

$$\bar{\rho}\sigma_{ij} = \bar{\rho}\left(\widetilde{u_i u_j} - \tilde{u}_i\tilde{u}_j\right), \qquad \beta_i = \frac{\partial\left(\bar{\tau}_{ij} - \check{\tau}_{ij}\right)}{\partial x_j} \quad (16)$$

respectively. Furthermore, the subgrid-scale terms occurring in the equation for the total resolved energy are

$$\alpha_1 = \tilde{u}_i \frac{\partial \bar{\rho}\sigma_{ij}}{\partial x_j}, \qquad \alpha_2 = \frac{1}{\gamma - 1}\frac{\partial}{\partial x_j}(\overline{pu_j} - \bar{p}\tilde{u}_j)$$

$$\alpha_3 = \overline{p\frac{\partial u_j}{\partial x_j}} - \bar{p}\frac{\partial \tilde{u}_j}{\partial x_j}, \qquad \alpha_4 = \overline{\tau_{ij}\frac{\partial u_i}{\partial x_j}} - \bar{\tau}_{ij}\frac{\partial \tilde{u}_i}{\partial x_j}$$

$$\alpha_5 = \frac{\partial}{\partial x_j}(\tilde{u}_i\bar{\tau}_{ij} - \tilde{u}_i\check{\tau}_{ij}), \quad \alpha_6 = \frac{\partial}{\partial x_j}(\bar{q}_j - \check{q}_j)$$

where α_1 is the SGS dissipation, and α_2 is the pressure-velocity correlation that resembles a turbulent heat flux and describes the contribution of the subgrid turbulence to the conduction of heat. The term α_3 is the pressure-dilatation correlation, and α_4 can be physically interpreted as SGS molecular dissipation [43].

The HPF Smagorinsky model [29,30] is based on the fixed-coefficient Smagorinsky model [44] and employs high-pass filtered quantities $H * \tilde{\boldsymbol{u}}$ instead of $\tilde{\boldsymbol{u}}$ for the computation of the turbulent eddy viscosity and the strain rate, where H is a suitable high-pass filter operator. The HPF Smagorinsky model then replaces $\bar{\rho}\sigma_{ij}$ in Eq. (14) by

$$\bar{\rho}\sigma_{ij} \approx m_{ij}^{\mathrm{HPF}} = -2\bar{\rho}\left(C^{\mathrm{HPF}}_{S,\omega_c}\Delta\right)^2 |S(H * \tilde{\boldsymbol{u}})| \cdot S_{ij}(H * \tilde{\boldsymbol{u}}) = -2\nu_t^{\mathrm{HPF}} S_{ij}(H * \tilde{\boldsymbol{u}}) \quad (17)$$

with the strain rate computed as

$$S_{ij}(H * \tilde{\boldsymbol{u}}) = \frac{1}{2}\left(\frac{\partial H * \tilde{u}_i}{\partial x_j} + \frac{\partial H * \tilde{u}_j}{\partial x_i} - \frac{2}{3}\delta_{ij}\frac{\partial H * \tilde{u}_k}{\partial x_k}\right)$$

and $|S(H * \tilde{\boldsymbol{u}})| = \sqrt{2S_{ij}(H * \tilde{\boldsymbol{u}})S_{ij}(H * \tilde{\boldsymbol{u}})}$. The filter width is chosen as $\Delta = (\Delta x_1 \Delta x_2 \Delta x_3)^{1/3}$.

Furthermore, the turbulent heat flux α_2 in the equation for the total resolved energy is modeled by an eddy-diffusivity ansatz based on the gradient of the high-pass filtered temperature:

$$\alpha_2 \approx \frac{\partial}{\partial x_j}\left(\frac{\nu_t^{\mathrm{HPF}}}{(\gamma - 1)Pr_t M^2}\frac{\partial (H * \tilde{T})}{\partial x_j}\right) \quad (18)$$

where the turbulent Prandtl number Pr_t is set to 0.7. For the SGS dissipation α_1, no additional model is required because it involves filtered quantities and the subgrid-scale stress tensor only. The other SGS terms, α_3 to α_6 and β_i, are neglected because they are expected to be smaller than the SGS terms that are modeled [43].

With suitable filters, high-pass filtered quantities are vanishingly small for smooth velocity profiles (e.g., low-order polynomials) and the corresponding SGS model contributions are evanescent. In our work, high-pass filtering is performed by subtracting low-pass filtered quantities from the unfiltered ones:

$$H * \tilde{u} = (I - G) * \tilde{u} \quad (19)$$

with the low-pass filter G defined by Eq. (5). As previously mentioned, the cutoff wave number of the explicit filter used herein is $\omega_c \approx 2\pi/3$. In Stolz et al. [30], the sensitivity of the simulation results employing the HPF Smagorinsky model to the model parameter C_0 was investigated. The effect of a variation by a factor of 3 (the squared quantity C_0^2 enters the model) is small for the HPF Smagorinsky model, whereas a significantly larger effect with the standard Smagorinsky model was found. To be consistent with other previous simulations, for example, turbulent and transitional

incompressible channel flow as well as compressible boundary layer flow [29,30,35], the model coefficient was set to $C_{S,\omega_c}^{\mathrm{HPF}} = 0.1$, employed in the previous studies.

IV. Forced Transition in a Supersonic Boundary Layer

The subharmonic transition process of a flat-plate boundary layer is simulated with a freestream Mach number of $M = 4.5$ and a Reynolds number of 10,000, based on the freestream velocity and initial displacement thickness, similar to the direct numerical simulation of Adams and Kleiser [10]. For the simulations, the temporal framework is adopted. As initial disturbance, the same perturbations as in the DNS [10] are employed, consisting of a second-mode instability with a streamwise wave number $\alpha = 2.52$ and amplitude $A_{2D} = 0.4\%$ (with respect to the maximum streamwise velocity fluctuation). To trigger the three-dimensional disturbances, random noise of low amplitude ($A_N = 10^{-4}$) is superimposed. The subharmonic secondary instability evolves from the noise in accordance with theory and leads to a staggered (subharmonic) Λ vortex pattern. For this case, it was concluded by Adams and Kleiser that, similar to incompressible flow, turbulence is generated via a cascade of vortices and detached shear layers forming with successively smaller scales.

The present reference DNS was performed using $160 \times 160 \times 301$ grid points throughout the whole simulation. Discretization is done with a sixth-order Padé scheme [37] in the wall-normal direction and a Fourier-spectral scheme in the wall-parallel directions, as explained in Sec. II. At the outer truncation plane, nonreflecting boundary conditions combined with a sponge layer were imposed to avoid reflections. The data of the present DNS compare well with those of Adams and Kleiser [10]. For the later stages of transition, only minor differences are visible, in comparison with the previous DNS by Mielke and Kleiser [11]. In particular, the prediction of the skin-friction coefficient, the shape factor, and the three-dimensional visualizations are in good agreement between the different DNS runs. We can therefore conclude that the resolution for the present DNS is sufficient to provide accurate reference data for the assessment of the different LES methods. We have chosen to recompute the DNS for the present work, because in the two previous DNS [10,11], the computational grid was changed during the course of the simulation to adapt to the necessary numerical resolution. These changes, however, include spatial interpolation from one grid to another, which could lead to slightly different numerical solutions. The slight difference in the evolution of the shape factor can be attributed to this interpolation procedure, which was not necessary in the present DNS. Moreover, we have used an increased resolution of $160 \times 160 \times 301$ grid points, compared with a maximum resolution of $128 \times 128 \times 240$ in Mielke and Kleiser and $128 \times 128 \times 191$ in Adams and Kleiser, to have reliable numerical reference data for comparison with LES.

For all LES, a deliberately low numerical resolution of $32 \times 32 \times 101$ has been used (only 1.3% of the grid points, compared with the DNS). Using an even coarser resolution the instability modes cannot be resolved anymore in the initial field, and large differences between LES and DNS can be observed. Furthermore, it was shown for other cases that with increasing numerical resolutions, the results of the LES converges toward the DNS [32,34]. Similarly, in the present flow case, the LES results converge toward the DNS results with an increased resolution. Because the LES results obtained with the comparably low resolution are already close to the filtered DNS results, LES data using higher resolution are not shown.

To ensure that consistent initial conditions are employed in both DNS and LES, the LES uses the initial field of the DNS after performing spectral interpolation in the periodic wall-parallel directions and B-spline interpolation in the wall-normal direction. All LES data are compared with the data obtained by filtering the present DNS results to the LES grid.

Although an LES consumed only about 10 CPU hours on a NEC SX-5 computer, the (temporal) DNS took 1000 hours using a highly optimized computer code. A spatial DNS would still cost an order of magnitude more and is therefore prohibitively expensive in terms of computer time.

A. Results of LES with the Approximate Deconvolution Model

We consider LES for the transitional supersonic boundary layers with ADM and different numerical schemes employed in the wall-normal direction (i.e., a sixth-order Padé scheme [37] and fourth-order centered explicit finite differences [39]). As mentioned previously, for all cases, a Fourier-collocation scheme was employed in the wall-parallel directions. Furthermore, an entropy-splitting approach is used in combination with the fourth-order finite differences, similar to the LES using the HPF Smagorinsky model, presented next (see also Sec. II).

All LES data obtained show very good agreement with DNS data for the skin-friction coefficient from the laminar well into the turbulent regime (see Fig. 1a). The skin-friction coefficient clearly peaks during the highly intermittent transitional phase, $t \approx 425$. Also visible in Fig. 1, the simulation with the fourth-order finite difference scheme for the wall-normal discretization (with and without entropy splitting) predicts transition slightly too early, by about 3.5% of the total time from initial disturbances ($t = 0$) until transition takes place. The shape factor $H_{12} = \delta_1/\delta_2$ (with $\delta_1 = \int_0^{\delta_0}(1-\rho u)\,\mathrm{d}z$ and $\delta_2 = \int_0^{\delta_0} \rho u(1-u)\,\mathrm{d}z$, δ_0 being the 99% boundary-layer thickness) is also predicted well, except for the fluctuations in the later stages of transition (see Fig. 1b). For the early turbulent phase, the shape factor was found to be in the range between 9 and 10, as expected from the experiments of Coles, as cited by Fernholz and Finley [45], and the DNS of Maeder et al. [46].

LES employing the Padé scheme in the wall-normal direction perform better than those with the explicit fourth-order finite

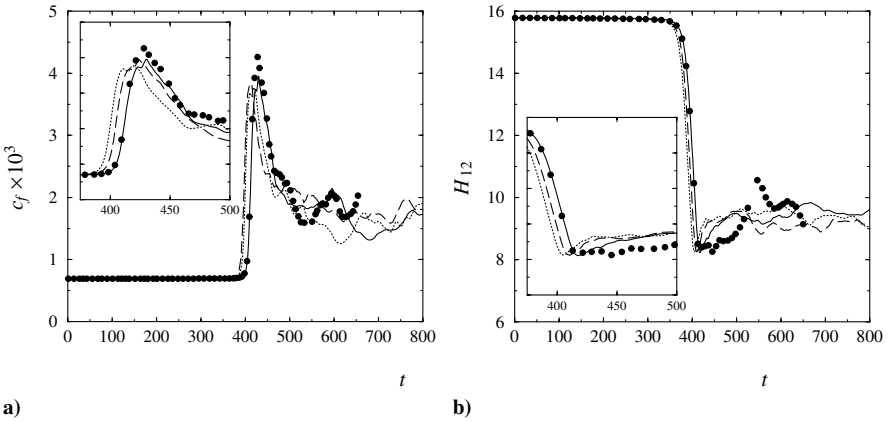

Fig. 1 Time evolution of integral quantities during transition showing a) skin-friction coefficient c_f and b) shape factor H_{12}; dots are filtered DNS and LES with ADM, solid lines are the sixth-order Padé scheme, dashed lines are the fourth-order centered explicit finite difference scheme in wall-normal direction, and dotted lines are the fourth-order scheme with entropy splitting.

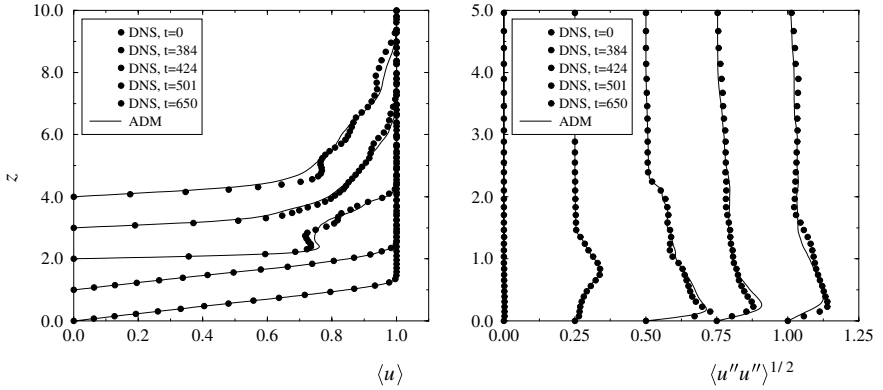

Fig. 2 Mean streamwise velocity profiles (left) and rms of Favre fluctuations u'' (right) at different stages of transition; lines are LES with ADM and dots are filtered DNS.

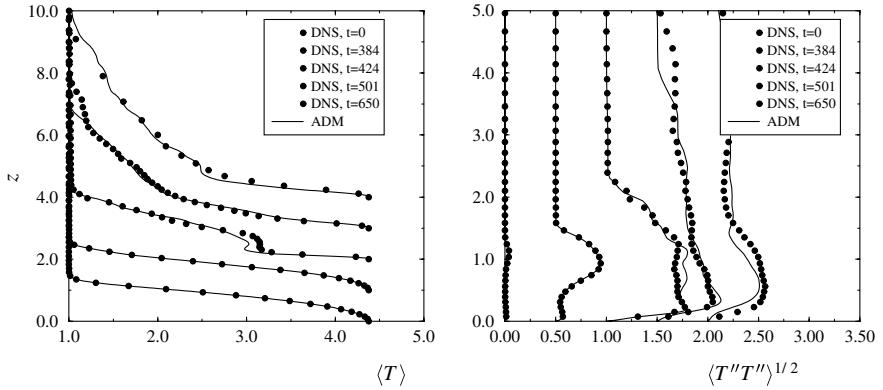

Fig. 3 Mean temperature profiles (left) and rms of Favre fluctuations T'' (right) at different stages of transition; lines are LES with ADM and dots are filtered DNS.

difference scheme at the present resolution. We show statistical results for mean profiles and fluctuations obtained with the combined Fourier-spectral/sixth-order Padé scheme (see Figs. 2 and 3). Statistical averaging is performed over the two homogeneous (i.e., streamwise and spanwise) directions and is denoted by $\langle\cdot\rangle$. The LES results are compared with the corresponding DNS data, indicated by symbols in Figs. 2 and 3 for different stages: before transition (initial field, $t = 0$), during transition ($t = 385$–502), and for the early turbulent phase ($t = 650$). The agreement of the mean streamwise velocity $\langle u\rangle$ and temperature $\langle T\rangle$ is very good for all stages. The root-mean-square (rms) values of the Favre fluctuations for the streamwise velocity $u'' = u - (\langle\rho u\rangle/\langle\rho\rangle)$ and temperature T'' are also very close to the DNS data for all stages of transition and the early turbulent phase. Note that in the turbulent stage, these data fluctuate considerably in time but no time averages are used herein. Furthermore, it should be kept in mind that averaging in wall-parallel planes is performed over much fewer points in the LES than in the DNS.

In addition to evaluating statistical quantities, we assess the capability of the LES to correctly predict instantaneous flow structures during the transition process. The physical mechanisms and flow structures have already been investigated in detail in earlier work [9,10]. In Fig. 4, we compare selected characteristic transitional structures predicted by LES using ADM with those present in the DNS, visualized with pressure isosurfaces. Three distinct stages within the breakup of the initial Y-shaped shear layer [9,10] are considered: the L1 roll-up of the Y shear layer at $t \approx 405$, the L3 roll-up of the Y shear layer at $t \approx 416$, and the LU1 roll-up at $t \approx 423$. These stages are the same as studied by Adams and Kleiser [10] and denote the first roll-up vortices (L1) near the legs of the Λ vortices, the third roll-up stage near the center of the legs (L3), and the cylinder-shaped vortices forming at the axis of symmetry of the Λ vortices (LU1). From Fig. 4, it can be concluded that LES with ADM captures these transitional structures very well, even on a comparably coarse grid. Similar conclusions were drawn by Schlatter et al.

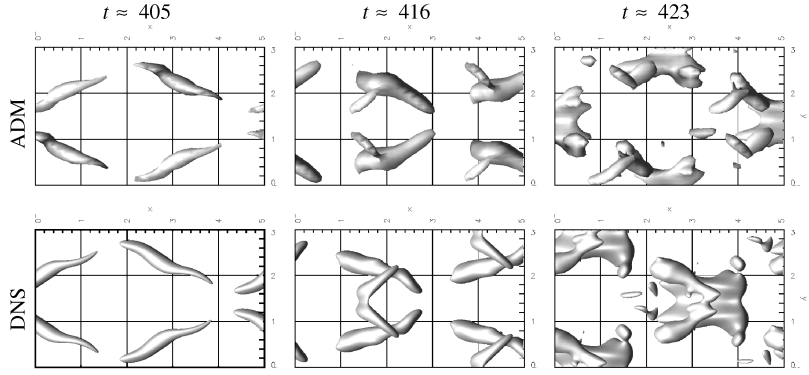

Fig. 4 Pressure isosurfaces (top view) at different stages of transition; LES with ADM with spectral/Padé scheme (top), DNS (bottom), L1 roll-up of the Y shear layer (left), L3 roll-up of the Y shear layer (center), and LU1 roll-up (right).

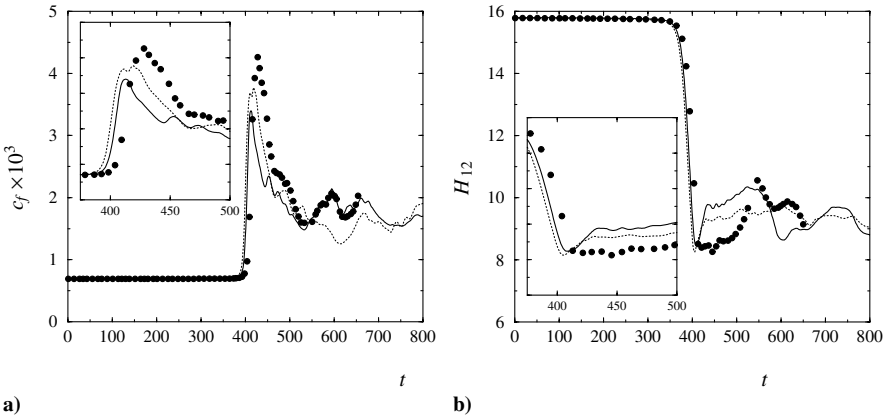

Fig. 5 Time evolution of integral quantities during transition showing a) skin-friction coefficient c_f and b) shape factor H_{12}; dots are filtered DNS and LES with fourth-order centered explicit finite difference scheme with entropy-splitting, solids lines are the HPF Smagorinsky model, and dotted lines are ADM.

[24,33] from detailed investigations of laminar-turbulent transition in incompressible channel flows.

B. Results of LES with the HPF Smagorinsky Model

For the LES applying the HPF Smagorinsky model, we used the numerical scheme proposed by Sandham et al. [38] based on fourth-order central finite differences [39] for the first and second derivatives (in both Stokes fluxes and the eddy-viscosity model) and an entropy-splitting approach. Simulations without entropy splitting or with the Padé scheme were found to be unstable for the entire time interval considered here on the present coarse LES grid.

The time evolution of the skin-friction coefficient c_f and shape factor H_{12} obtained from the LES with the HPF Smagorinsky model is shown in Fig. 5, and the profiles of the mean velocity and mean temperature as well as the corresponding fluctuations are depicted in Figs. 6 and 7, respectively. The skin-friction peak obtained with the HPF Smagorinsky model is slightly underpredicted and, similar to the simulation with ADM using the fourth-order finite difference scheme, transition is predicted slightly too early, by about $\Delta t \approx 7$ or 3.5% of the total time interval until transition. For this reason, the profiles of mean velocity and temperature and the corresponding fluctuations in the rapidly evolving transition process are shown at times earlier than in the DNS, by about $\Delta t = 7$ (see, for example, Figs. 6 and 7). Mean quantities and fluctuations of the velocity and temperature are again predicted quite well. We conclude that it is possible to compute high-speed transitional boundary-layer flows by coarse-grid LES using the HPF Smagorinsky model. The same

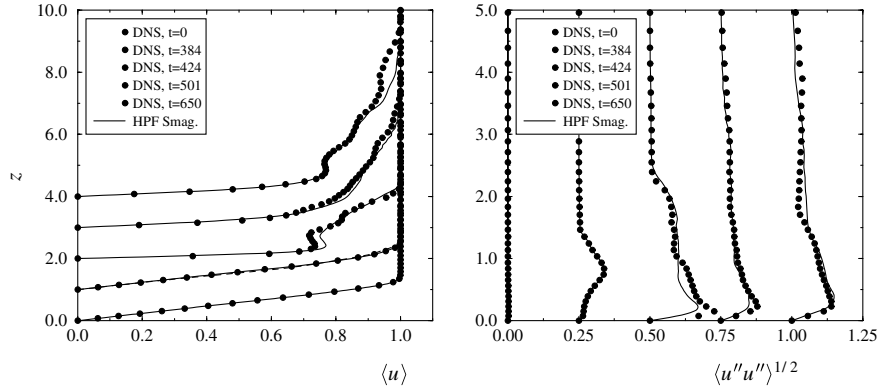

Fig. 6 Mean streamwise velocity profiles (left) and rms of Favre fluctuations u'' (right) at different stages of transition; lines are LES with the HPF Smagorinsky model (shifted in time by $\Delta t \approx 7$) and dots are filtered DNS.

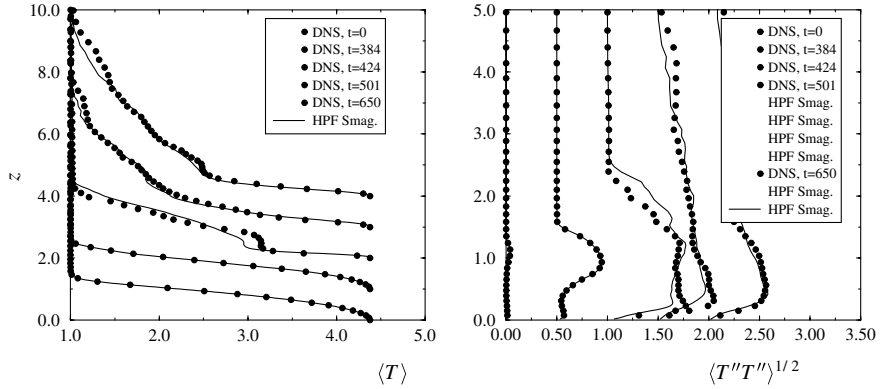

Fig. 7 Mean temperature profiles (left) and rms of Favre fluctuations T'' (right) at different stages of transition; lines are LES with the HPF Smagorinsky model (shifted in time by $\Delta t \approx 7$) and dots are filtered DNS.

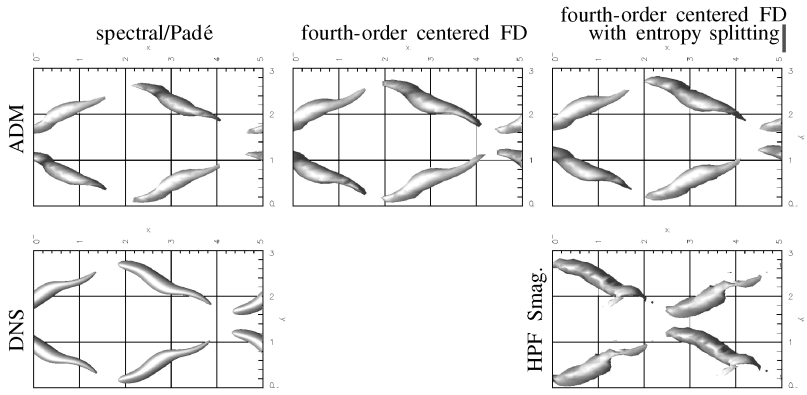

Fig. 8 Pressure isosurfaces (top-view) for the LU1 roll-up stage at $c_f \approx 0.00115$. LES with ADM with spectral/Padé scheme (top left, $t \approx 405$), LES with ADM with fourth-order FD scheme (top center, $t \approx 400$), ADM fourth-order FD scheme with entropy splitting (top right, $t \approx 395$), DNS (bottom left, $t \approx 405$), and LES with HPF Smagorinsky model (bottom right, $t \approx 398$).

conclusion was already drawn for incompressible channel flow by Stolz et al. [30]. Note that for the HPF Smagorinsky model, a fixed model coefficient could be used throughout the whole simulation and no dynamic procedure was necessary.

With the HPF Smagorinsky model, structures of the earlier transitional stages can be predicted accurately (see Fig. 8). However, the flow structures present in the transitional process for later stages cannot be captured with the same accuracy as with using the ADM. For example, in the L3 roll-up of the Y shear layer, the LU1 roll-up can clearly be observed in both the LES with ADM and the DNS. This is mainly due to the SGS model, as can be seen from Fig. 8, in which the LU1 roll-up is depicted for the simulation with the HPF Smagorinsky model and compared with results of LES with ADM and different numerical schemes. The flow structures predicted with the HPF Smagorinsky model are substantially more noisy than for all simulations with ADM, and they break down quickly, without showing the correct physical evolution for the latest stages of development.

V. Conclusions

The forced subharmonic transition process of a $M = 4.5$ flat-plate boundary layer was simulated successfully by means of LES using the approximate deconvolution model [26–28] and the high-pass filtered Smagorinsky model [29–31]. LES results were compared with data obtained from a fully resolved DNS performed for this purpose. The simulations show that both subgrid-scale models can be employed for the computation of transitional flows without any adaptation. This confirms previous findings for transition in incompressible channel flow with ADM [32] and the HPF Smagorinsky model [30].

Mean flow data of LES with both SGS models agree well with DNS data during transition, up to the turbulent stage. Moreover, it was shown that ADM is also able to capture typical instantaneous flow structures during the transition process. To separate modeling and numerical discretization issues, we also investigated the influence of the finite difference scheme on simulations with ADM. It appears that for a correct representation of flow structures, the SGS model is more important than the specific high-order numerical scheme.

Acknowledgments

This work was partially supported by the European Space Agency (ESA), contract no. 17592/03/NL/SFe. Calculations have been performed at the Swiss National Supercomputing Centre (CSCS), Manno, Switzerland.

References

[1] Mack, L. M., "Boundary-Layer Linear Stability Theory," AGARD, Rept. 709, Neuilly sur-Seine, France, 1984, pp. 3.1–3.81.

[2] Mack, L. M., "On the Inviscid Acoustic-Mode Instability of Supersonic Shear Flows, Part 1: Two-Dimensional Waves," *Theoretical and Computational Fluid Dynamics*, Vol. 2, No. 2, 1990, pp. 97–123.

[3] Ng, L. L., and Erlebacher, G., "Secondary Instabilities in Compressible Boundary Layers," *Physics of Fluids A*, Vol. 4, No. 4, 1992, pp. 710–726.

[4] Forgoston, E., and Tumin, A., "Initial-Value Problem for Three-Dimensional Disturbances in a Compressible Boundary Layer," *Physics of Fluids*, Vol. 17, No. 084106, 2005, pp. 1–14.

[5] Saric, W. S., Reshotko, E., and Arnal, D., "Hypersonic Laminar-Turbulent Transition," *Hypersonic Experimental and Computational Capability, Improvement and Validation*, AGARD Rept. AR-319 Vol. 2, Neuilly sur-Seine, France, 1998, pp. 2.1–2.27.

[6] Guo, Y., Adams, N. A., Sandham, N. D., and Kleiser, L., "Numerical Simulation of Supersonic Boundary Layer Transition," *Application of Direct and Large-Eddy Simulation to Transition to Turbulence*, AGARD Rept. CP-551, Neuilly sur-Seine, France, 1994, pp. 13.1-13.12.

[7] Husmeier, F., Mayer, C. S. J., and Fasel, H. F., "Investigation of Transition of Supersonic Boundary Layers at Mach 3 Using DNS," AIAA Paper 2005-0095, 2005.

[8] Rempfer., D., "Low-Dimensional Modeling and Numerical Simulation of Transition in Simple Shear Flows," *Annual Review of Fluid Mechanics*, Vol. 35, 2003, pp. 229–265.

[9] Adams, N. A., "Numerische Simulation von Transitionsmechanismen in Kompressiblen Grenzschichten," Ph.D. Thesis, Technische Univ. München, Munich, Germany, 1993; also DLR, German Aerospace Center, Rept. DLR-FB 93-29, Göttingen, Germany, (in German).

[10] Adams, N. A., and Kleiser, L., "Subharmonic Transition to Turbulence in a Flat Plate Boundary Layer at Mach Number 4.5," *Journal of Fluid Mechanics*, Vol. 317, June 1996, pp. 301–335.

[11] Mielke, C., and Kleiser, L., "Investigation of the Late Stages of Transition to Turbulence in a Mach 4.5 Boundary Layer," *Computation and Visualization of Three-Dimensional Vortical and Turbulent Flows*, Vol. 64, Notes on Numerical Fluid Mechanics, edited by R. Friedrich and P. Bontoux, Vieweg–Verlag, Braunschweig, Germany, 1998, pp. 329–338.

[12] Germano, M., Piomelli, U., Moin, P., and Cabot, W. H., "A Dynamic Subgrid-Scale Eddy Viscosity Model," *Physics of Fluids A*, Vol. 3, No. 7, 1991, pp. 1760–1765.

[13] Meneveau, C., Lund, T. S., and Cabot, W. H., "A Lagrangian Dynamic Subgrid-Scale Model of Turbulence," *Journal of Fluid Mechanics*, Vol. 319, July 1996, pp. 353–385.

[14] Schlatter, P., "Large-Eddy Simulation of Transition and Turbulence in Wall-Bounded Shear Flow," Ph.D. Thesis, No. 16000, Eidgenössische Technische Hochschule Zürich, Zürich, Switzerland, 2005; also available at http://e-collection.ethbib.ethz.ch.

[15] El-Hady, N., and Zang, T. A., "Large-Eddy Simulation of Nonlinear Evolution and Breakdown to Turbulence in High-Speed Boundary Layers," *Theoretical and Computational Fluid Dynamics*, Vol. 7, No. 3, 1995, pp. 217–240.

[16] Zang, Y., Street, R. L., and Koseff, J. H., "A Dynamic Mixed Subgrid-Scale Model and Its Application to Turbulent Recirculating Flows," *Physics of Fluids A*, Vol. 5, No. 12, 1993, pp. 3186–3196.

[17] Normand, X., and Lesieur, M., "Direct and Large-Eddy Simulations of Transition in the Compressible Boundary Layer," *Theoretical and Computational Fluid Dynamics*, Vol. 3, No. 4, 1992, pp. 231–252.

[18] Métais, O., and Lesieur, M., "Spectral Large-Eddy Simulations of Isotropic and Stably Stratified Turbulence," *Journal of Fluid Mechanics*, Vol. 239, June 1992, pp. 157–194.
[19] Ducros, F., Comte, P., and Lesieur, M., "Large-Eddy Simulation of Transition to Turbulence in a Boundary Layer Developing Spatially over a Flat Plate," *Journal of Fluid Mechanics*, Vol. 326, 1996, pp. 1–36.
[20] Shan, H., Jiang, L., and Liu, C., "Large Eddy Simulation of Flow Transition in a Compressible Flat-Plate Boundary Layer at Mach 4.5," *International Journal of Computational Fluid Dynamics*, Vol. 13, No. 1, 1999, pp. 25–41.
[21] Teramoto, S., "Large-Eddy Simulation of Transitional Boundary Layer with Impinging Shock Wave," *AIAA Journal*, Vol. 43, No. 11, 2005, pp. 2354–2363.
[22] Kleiser, L., and Zang, T. A., "Numerical Simulation of Transition in Wall-Bounded Shear Flows," *Annual Review of Fluid Mechanics*, Vol. 23, 1991, pp. 495–537.
[23] Fasel, H. F., "Numerical Simulation of Instability and Transition in Boundary Layer Flows," *Third IUTAM Symposium on Laminar-Turbulent Transition*, edited by D. Arnal and R. Michel, Springer, Berlin, 1990, pp. 587–598.
[24] Schlatter, P., Stolz, S., and Kleiser, L., "LES of Spatial Transition in Plane Channel Flow," *Journal of Turbulence*, Vol. 7, No. 33, 2006, pp. 1–24.
[25] Brandt, L., Schlatter, P., and Henningson, D. S., "Transition in Boundary Layers Subject to Free-Stream Turbulence," *Journal of Fluid Mechanics*, Vol. 517, 2004, pp. 167–198.
[26] Stolz, S., and Adams, N. A., "An Approximate Deconvolution Procedure for Large-Eddy Simulation," *Physics of Fluids*, Vol. 11, No. 7, 1999, pp. 1699–1701.
[27] Stolz, S., Adams, N. A., and Kleiser, L., "An Approximate Deconvolution Model for Large-Eddy Simulation with Application to Incompressible Wall-Bounded Flows," *Physics of Fluids*, Vol. 13, No. 4, 2001, pp. 997–1015.
[28] Stolz, S., Adams, N. A., and Kleiser, L., "The Approximate Deconvolution Model for LES of Compressible Flows and Its Application to Shock-Turbulent-Boundary-Layer Interaction," *Physics of Fluids*, Vol. 13, No. 10, June 2001, pp. 2985–3001.
[29] Stolz, S., "High-Pass Filtered Eddy-Viscosity Models for Large-Eddy Simulations of Compressible Wall-Bounded Flows," *Journal of Fluids Engineering*, Vol. 127, No. 4, 2005, pp. 666–673.
[30] This reference is missing a required coden or issn tag.Stolz, S., Schlatter, P., and Kleiser, L., "High-Pass Filtered Eddy-Viscosity Models for Large-Eddy Simulations of Transitional and Turbulent Flow," *Physics of Fluids*, Vol. 17, No. 065103, 2005, pp. 1–14.
[31] This reference is missing a required coden or issn tag.Vreman, A. W., "The Filtering Analog of the Variational Multiscale Method in Large-Eddy Simulation," *Physics of Fluids*, Vol. 15, No. 8, 2003, pp. L61-L64.
[32] Schlatter, P., Stolz, S., and Kleiser, L., "LES of Transitional Flows Using the Approximate Deconvolution Model," *International Journal of Heat and Fluid Flow*, Vol. 25, No. 3, 2004, pp. 549–558.
[33] Schlatter, P., Stolz, S., Kleiser, L., "Applicability of LES Models for Prediction of Transitional Flow Structures," *Sixth IUTAM Symposium on Laminar-Turbulent Transition*, edited by R. Govindarajan, Springer, Berlin, 2005, pp. 323–328.
[34] This reference is missing a required coden or issn tag.Stolz, S., and Adams, N. A., "Large-Eddy Simulation of High-Reynolds-Number Supersonic Boundary Layers Using the Approximate Deconvolution Model and a Rescaling and Recycling Technique," *Physics of Fluids*, Vol. 15, No. 8, 2003, pp. 2398–2412.
[35] Schlatter, P., and Stolz, S., and Kleiser, L., "Evaluation of High-Pass Filtered Eddy-Viscosity Models for Large-Eddy Simulation of Turbulent Flows," *Journal of Turbulence*, Vol. 6, No. 5, 2005, pp. 1–21.
[36] Piomelli, U., Zang, T. A., Speziale, C. G., and Hussaini, M. Y., "On the Large-Eddy Simulation of Transitional Wall-Bounded Flows," *Physics of Fluids A*, Vol. 2, No. 2, 1990, pp. 257–265.
[37] Lele, S. K., "Compact Finite Difference Schemes with Spectral-Like Resolution," *Journal of Computational Physics*, Vol. 103, No. 1, 1992, pp. 16–42.
[38] Sandham, N. D., Li, W., and Yee, H. C., "Entropy Splitting for High-Order Numerical Simulation of Compressible Turbulence," *Journal of Computational Physics*, Vol. 178, No. 2, 2002, pp. 307–322.
[39] Carpenter, M. H., Gottlieb, J., and Gottlieb, D., "A Stable and Conservative Interface Treatment of Arbitrary Spatial Accuracy," *Journal of Computational Physics*, Vol. 148, No. 2, 1999, pp. 341–365.
[40] Gerritsen, M., and Olsson, P., "Designing an Efficient Solution Strategy for Fluid Flows," *Journal of Computational Physics*, Vol. 129, No. 2, 1996, pp. 245–262.
[41] Harten, A., "On the Symmetric Form of Systems of Conservation Laws with Entropy," *Journal of Computational Physics*, Vol. 49, No. 1, 1983, pp. 151–164.
[42] Williamson, J. H., "Low-Storage Runge-Kutta Schemes," *Journal of Computational Physics*, Vol. 35, No. 1, 1980, pp. 48–56.
[43] Vreman, A. W., "Direct and Large-Eddy Simulation of the Compressible Turbulent Mixing Layer," Ph.D. Thesis, Univ. of Twente, Enschede, The Netherlands, 1995.
[44] Smagorinsky, J., "General Circulation Experiments with the Primitive Equations," *Monthly Weather Review*, Vol. 91, No. 3, 1963, pp. 99–164.
[45] Fernholz, H. H., and Finley, P. J., "A Critical Compilation of Compressible Turbulent Boundary Layer Data," AGARD, AGARDograph 223, Neuilly sur-Seine, France, 1977.
[46] Maeder, T., Adams, N. A., and Kleiser, L., "Direct Simulation of Turbulent Supersonic Boundary Layers by an Extended Temporal Approach," *Journal of Fluid Mechanics*, Vol. 429, Feb. 2001, pp. 187–216.

D. Gaitonde
Associate Editor